

CRISPR

Csx28 is a membrane pore that enhances CRISPR-Cas13b-dependent antiphage defense

Arica R. VanderWal^{1,2,††}, Jung-Un Park³, Bogdan Polevoda^{1,2}, Julia K. Nicosia^{1,2}, Adrian M. Molina Vargas^{1,2}, Elizabeth H. Kellogg³, Mitchell R. O'Connell^{1,2,*}

Type VI CRISPR-Cas systems use RNA-guided ribonuclease (RNase) Cas13 to defend bacteria against viruses, and some of these systems encode putative membrane proteins that have unclear roles in Cas13-mediated defense. We show that Csx28, of type VI-B2 systems, is a transmembrane protein that assists to slow cellular metabolism upon viral infection, increasing antiviral defense. High-resolution cryo-electron microscopy reveals that Csx28 forms an octameric pore-like structure. These Csx28 pores localize to the inner membrane *in vivo*. Csx28's antiviral activity *in vivo* requires sequence-specific cleavage of viral messenger RNAs by Cas13b, which subsequently results in membrane depolarization, slowed metabolism, and inhibition of sustained viral infection. Our work suggests a mechanism by which Csx28 acts as a downstream, Cas13b-dependent effector protein that uses membrane perturbation as an antiviral defense strategy.

Type VI CRISPR-Cas systems contain a single effector protein, Cas13 (formerly C2c2), which when assembled with CRISPR RNA (crRNA) forms a crRNA-guided RNA-targeting complex (1, 2). Cas13 possesses a pre-crRNA processing nuclease for mature crRNA formation, as well as a target nuclease that cleaves both foreign and host RNA transcripts indiscriminately (3); this activity has been shown in several cases to lead to cellular dormancy upon targeting plasmids or phage transcripts during infection (1, 4).

Recently, two accessory genes, *csx27* and *csx28*, were found to modulate the antiphage defense activity of specific Cas13b-containing CRISPR systems (type VI-B) when challenged with MS2 single-stranded RNA (ssRNA) phage (5) and have been predicted to contain transmembrane-spanning regions by means of a transmembrane protein-prediction algorithm, transmembrane prediction using hidden Markov models (TMHMM) (5, 6). In addition, Csx28 was predicted to potentially contain a divergent higher eukaryotic and prokaryotic nucleotide-binding (HEPN) motif (5, 6), which has been hypothesized to act as an RNA nuclease (3, 6–8); however, the relevance of any of these predicted features is unclear.

We focus on Cas13b- and Csx28-containing type VI-B2 systems and show that during Cas13b-crRNA guided cleavage of phage mRNA during infection, Csx28 and its membrane-embedded

pore-like structure help to slow cellular metabolism, and that this activity drastically increases antiviral defense. Our work suggests a mechanism by which CRISPR-Cas proteins cooperate to restrict phage propagation through membrane perturbation, implying a more general link between cytoplasmic CRISPR-Cas nucleic acid detection and membrane perturbation as an antiviral defense strategy.

Csx28 is required for optimal interference against λ phage and requires an active, phage-targeting Cas13b

We implemented a phage interference system to understand how Csx28 contributes to antiphage defense. Because most type VI CRISPR-Cas system spacers align to transcripts from double-stranded DNA (dsDNA) phage and prophage genomes (in many cases, lysogenic lambdoid phages) (5, 9–12), we focused on using the type VI-B2 system from *Prevotella buccae* ATCC 33574 (Fig. 1A) and λ phage in a heterologous, plasmid-based *Escherichia coli* system (Fig. 1, B and C). Phage susceptibility was first assessed with λ -phage efficiency of plating (EOP) assays, and we found that whereas Cas13b-crRNA-1 and Cas13b-crRNA-2 provided modest protection to phage infection, the presence of Csx28 substantially enhanced both Cas13b-crRNA-1- and Cas13b-crRNA-2-mediated antiphage activities (Fig. 1D). Csx28-mediated enhancement of antiphage defense requires the presence of a nuclease active, λ -targeting Cas13 because Csx28-mediated enhancement is completely abrogated by (i) the absence of Cas13 (Δ Cas13), (ii) the absence of an λ -targeting crRNA (Δ crRNA), (iii) scrambling of the λ -targeting crRNA spacer sequence, and (iv) mutation of the active-site residues of Cas13's HEPN nuclease (Cas13b^{dHEPN}) (Fig. 1D and fig. S1). These results recapitulate a similar Csx28 antiphage defense effect observed in MS2 ssRNA phage experiments (5). We additionally observed that enhanced anti-MS2 phage de-

fense strictly requires a targeting Cas13b, because Csx28 alone does not offer any defense (fig. S2).

We next monitored bacterial growth rates after phage infection (Fig. 1, E to H). Cas13b-crRNA-1 and -crRNA-2 alone can respond to λ -phage infection at a low multiplicity of infection (MOI) of 0.2, which results in delayed lysis at the population level, cessation of growth, and a loss of cell density, suggesting a Cas13b-mediated-dormancy phenotype (Fig. 1, E and F) as previously observed with Cas13a (4). By contrast, upon phage infection, Cas13b-crRNA-3 and Cas13b- Δ crRNA respond similarly to untransformed *E. coli* (Fig. 1, G and H). In the case of Cas13b-crRNA-1 and -crRNA-2, the addition of Csx28 can rescue this defect, resulting in a continued albeit slower growth rate relative to uninfected cells. Whereas Csx28's enhancement effect is muted at a higher MOI (MOI of 2), Cas13b-crRNA-1 in the presence of Csx28 can still resist cell death after λ -phage infection (fig. S3, A to D). To confirm that this response is not due to the indirect growth effects of protein expression or antibiotics, we demonstrated that strains containing Cas13b^{dHEPN}-crRNA1 and either Csx28 or an empty vector respond very similarly to untransformed *E. coli* (fig. S3, E and F). We also confirmed that these effects are not due to changes in cell morphology or lysogen formation (fig. S4, A and B, and supplementary text). These findings suggest that Csx28 is acting to prevent phage propagation and/or cell lysis, thereby enabling the cultures to continue to increase in cell density.

To determine at what stage of lytic λ -phage infection Csx28 is acting to enhance defense, we carried out efficiency of center of infection (ECOI) assays and phage accumulation assays. The ECOI assays revealed that Cas13b-crRNA-1 alone resulted in ~18.5% of infected cells releasing at least one infectious virion and that the addition of Csx28 to Cas13b-crRNA-1 cultures (but not Csx28 alone) further reduced the release of phage to only ~3% of infected cells, indicating that Csx28 can enhance Cas13b defense by limiting the number of initially infected cells releasing phage progeny (Fig. 1I). To observe phage accumulation within our system, we determined phage titer over time and found a significant reduction of phage numbers per milliliter when hosts were protected with Cas13b and Csx28 compared with untransformed *E. coli* or hosts containing only Cas13b, with further amplification of this protective effect across subsequent time points (Fig. 1J). This result indicates that an actively targeting Cas13b is required for Csx28's robust enhancement of antiphage defense against a dsDNA phage, and that this is achieved by Csx28 inducing a bacteriostatic phenotype that helps prevent the establishment and maintenance of λ -phage infection.

¹Department of Biochemistry and Biophysics, School of Medicine and Dentistry, University of Rochester, Rochester, NY, USA. ²Center for RNA Biology, University of Rochester, Rochester, NY, USA. ³Department of Molecular Biology and Genetics, Cornell University, Ithaca, NY, USA. ⁴Department of Biomedical Genetics, School of Medicine and Dentistry, University of Rochester, Rochester, NY, USA.

*Corresponding author. Email: mitchell_oconnell@urmc.rochester.edu

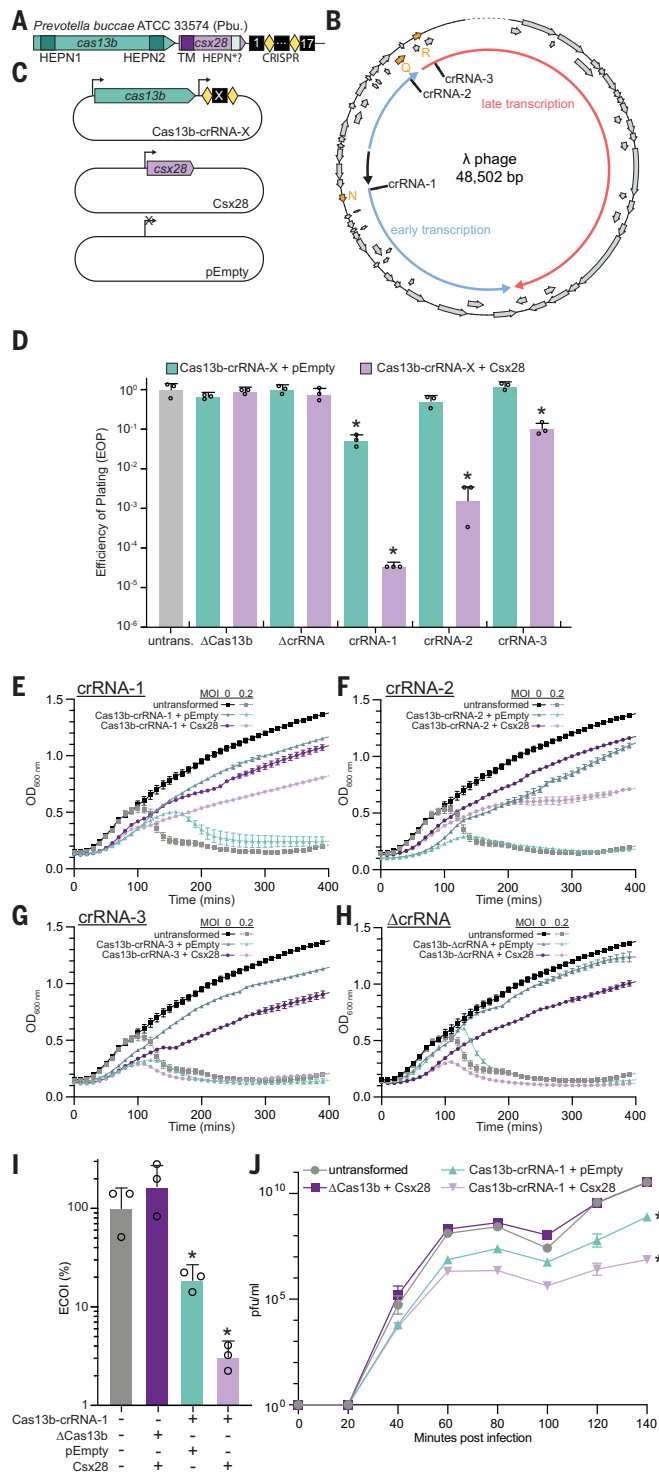
†Present address: Department of Molecular Biology, School of Biological Sciences, University of California San Diego, La Jolla, CA, USA.

‡Present address: Howard Hughes Medical Institute, University of California San Diego, La Jolla, CA, USA.



Fig. 1. Csx28 enhances Cas13b-mediated immunity against λ phage by inducing a slow-growing phenotype that helps prevent the establishment and maintenance of infection.

(A) Schematic of the type VI-B2 CRISPR-Cas system from *P. buccae*. (B) Schematic of the λ -phage genome in its circular form, showing the location of crRNA-1 to crRNA-3 target sites. bp, base pair. (C) Plasmid schematics for phage interference experiments in which Cas13b and Csx28 are expressed on two separate plasmids. Cas13b-crRNA-X also contains a synthetic CRISPR-Cas array. (D) EOP assays measuring λ -phage infection susceptibility of untransformed (untrans.) *E. coli* or of *E. coli* carrying the indicated plasmids. (E to H) Growth curves of *E. coli* carrying the indicated plasmids, as measured by means of OD₆₀₀ (optical density at 600 nm) after the addition of λ phage at an MOI of 0.2. (I) ECOL assays measuring λ -phage infective center formation of *E. coli* strains carrying the indicated plasmids infected with λ phage at an MOI of 0.1. (J) Phage growth assays measuring the λ -phage production over time for *E. coli* strains carrying the indicated plasmids infected with λ phage at an MOI of 0.1. Data in (D) through (J) are shown as mean \pm SEM for three biological replicates. One-way analysis of variance (ANOVA) and Dunnett's multiple comparisons test was used for data in (D) and (I); repeated measures one-way ANOVA was calculated by using the Geisser-Greenhouse correction and Dunnett's multiple comparisons test was used for data in (J), comparing strains with plasmids to the untransformed control. No significance was detected, unless indicated (* $p \leq 0.05$).



maltoside (DDM) solubilization, suggesting that it may be membrane associated in vivo. Size exclusion chromatography (SEC) indicated that DDM-solubilized Csx28 was forming two discrete, nonexchanging oligomers of different sizes in solution (henceforth referred to as light and heavy fractions; fig. S5). SEC coupled with static light scattering (SEC-SLS) showed that the heavy fraction of Csx28 has an average experimental mass of \sim 170 kDa (the molecular weight of a Csx28 monomer is \sim 21 kDa), implying an octameric complex. On the front tail of the heavy-fraction peak, Csx28 octamers are dynamically exchanging to form larger 16-mer species (Fig. 2A and fig. S6). Because the light fraction co-elutes with empty DDM micelles, calculating an accurate molecular mass was not possible; consequently we used in vitro cross-linking and observed that the light fraction of Csx28 is monomeric in solution, and that the heavy fraction predominately forms Csx28 octamers, in line with the SEC-SLS experiments (fig. S7).

We determined the structure of Csx28 (heavy fraction) in a DDM micelle to an estimated global resolution of 3.65 Å by using cryo-electron microscopy (cryo-EM) (Fig. 2B, fig. S8, and table S1). Two-dimensional (2D) class averages indicated the presence of eightfold symmetry, with the imposition of C8 symmetry resulting in a high-resolution cryo-EM reconstruction (Fig. 2B). The resulting reconstruction is a homo-octamer with an eightfold symmetry about a central pore; a nearly full-length model, corresponding to amino acid residues 19 to 171, was built into the asymmetric unit (full-length Csx28 comprises 177 amino acids). The structure can be divided into two distinct regions: a partially unresolved single N-terminal α helix embedded in a DDM micelle [matching the membrane topology prediction generated by TMHMM (13)] and a well-ordered C-terminal cytoplasmic domain (Fig. 2, B and C). As commonly observed, the DDM micelle appears as a diffuse spherical density (Fig. 2B); the remaining low-resolution features apparent in a low-pass filtered version of the cryo-EM map indicate how Csx28's N-terminal transmembrane helix may traverse the lipid bilayer. The 3D class averages recapitulate our SEC-SLS data, with the two major classes forming octamers and the minor class forming a 16-mer (fig. S8). The central pore has a minimal diameter of \sim 10 Å, similar to the diameters observed in many large-pore channels (for example, connexin gap junction channels), which can permeate ions and in some cases small metabolites, but it is likely too small for the passage of small proteins, as is seen with most phage holins or gasdermins (74). Each protomer is organized as a four-helix bundle (α 1 to α 4), with the N-terminal helices (α 1 and α 2) lining the inside of the pore and the two C-terminal

Cryo-EM reveals that Csx28 forms an octameric membrane-pore structure

To further understand how Csx28 is functioning to enhance Cas13b-mediated antiphage

defense, we expressed and purified recombinant Csx28 from *E. coli*. We found that Csx28 was insoluble in standard cytosolic protein-purification buffers and required dodecyl

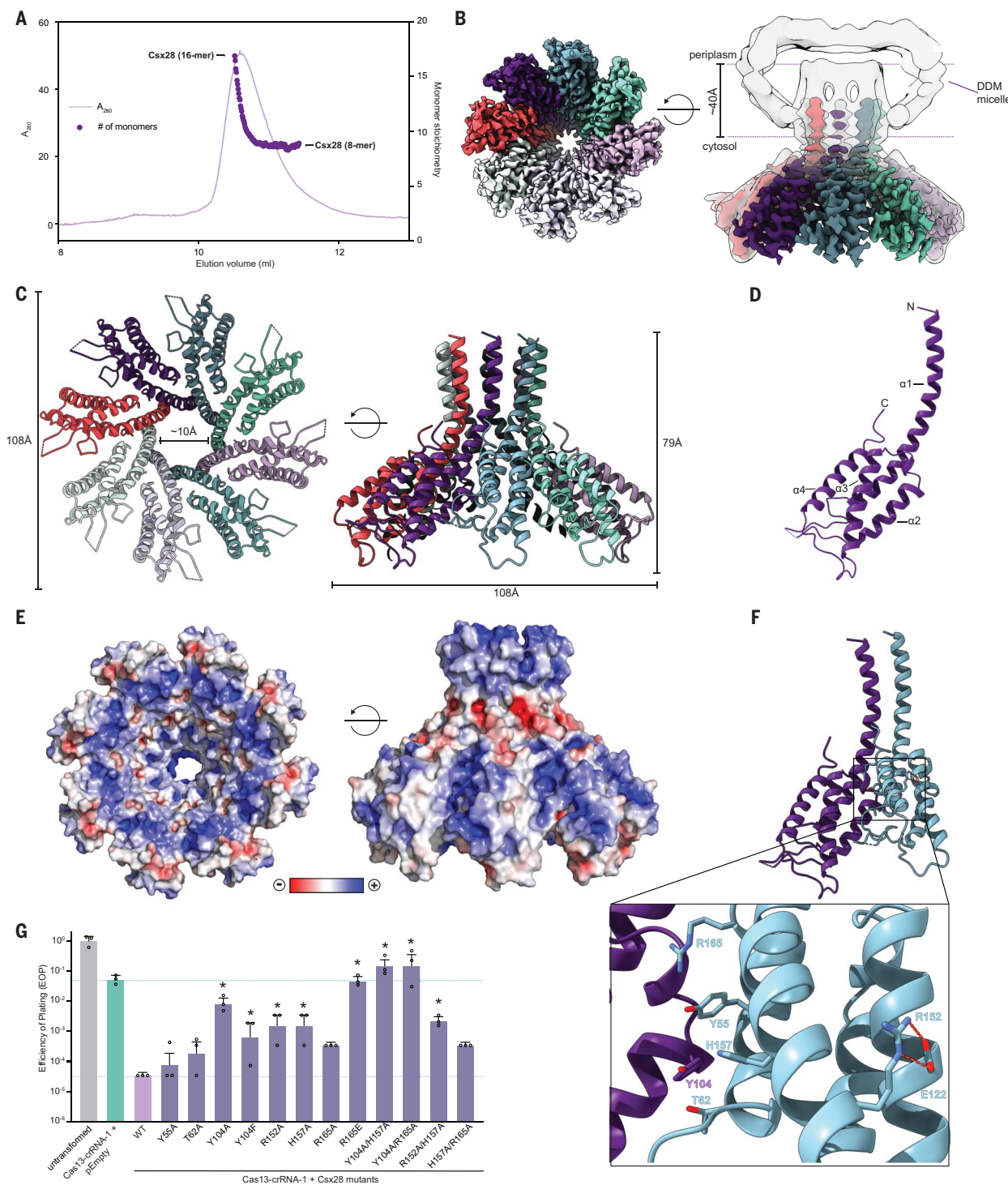


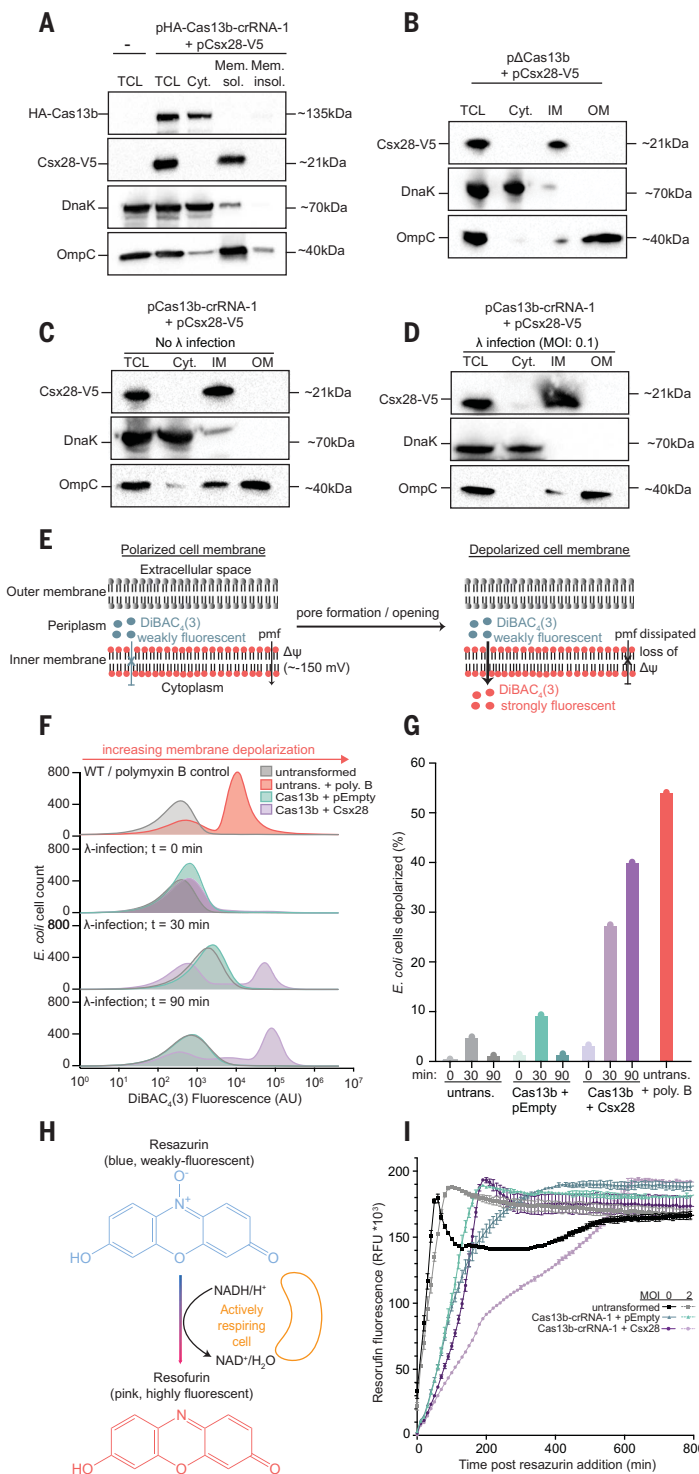
Fig. 2. Cryo-EM reveals that Csx28 forms an octameric detergent-embedded pore-like structure with a distinctive protomer interface. (A) SEC-SLS analysis of Csx28 heavy fraction. See fig. S5 for full three-detector traces of Csx28 and a bovine serum albumin (BSA) standard. A_{280} , absorbance units at 280 nm. (B) High-resolution (3.65-Å) cryo-EM reconstruction of Csx28 (each protomer is distinctively colored) embedded in a DDM micelle, which is displayed as a composite high-resolution cryo-EM map superimposed with an 8-Å low-pass filtered version of the same map to display lower-resolution features, such as the DDM micelle and transmembrane helices. (C) Bottom and side views of the atomic model of the Csx28 octamer. The dimensions of the octamer and the diameter at the constriction of the pore are shown. (D) Atomic model of an isolated Csx28 protomer with each helix

of the four α -helical bundle labeled. (E) Electrostatic surface representations of the bottom and side of Csx28. The red-to-blue color gradient represents negative to positive electrostatic potential ($\pm 5 \text{ kT/e}$). (F) A magnified view of the Csx28 protomer-protomer interface. Amino acid residues of interest are shown as sticks and labeled. (G) EOP assays measuring the effect of amino acid mutations at the Csx28 protomer-protomer interface on λ -phage infection susceptibility of *E. coli* strains carrying the indicated plasmids. Data are shown as mean \pm SEM for three biological replicates. Statistical significance was calculated with one-way ANOVA and Dunnett's multiple comparisons test, comparing mutant Csx28 strains to wild-type (WT) Csx28. No significance was detected, unless indicated (* $p \leq 0.05$). Single-letter abbreviations for the amino acid residues are as follows: A, Ala; E, Glu; F, Phe; H, His; R, Arg; T, Thr; and Y, Tyr.

Fig. 3. Csx28 localizes to the inner membrane in *E. coli* regardless of Cas13b expression or λ -phage infection and is required for membrane depolarization and a loss of metabolic activity upon Cas13b sensing of λ -phage infection. (A) Western blot to detect the localization of Cas13 and Csx28 in cytosolic versus detergent-soluble and detergent-insoluble fractions obtained from *E. coli* expressing HA-tagged Cas13b-crRNA1 and/or V5-tagged Csx28. TCL, total cell lysate; Cyt., cytosolic fraction; Mem. sol., membrane soluble fraction; Mem. insol., membrane insoluble fraction.

(B) Western blot to detect the localization of Csx28 in inner- or outer-membrane fractions from *E. coli* expressing Δ Cas13b and V5-tagged Csx28. **(C and D)** Western blot to detect the localization of Csx28 in inner- or outer-membrane fractions from *E. coli* expressing Cas13b-crRNA1 and V5-tagged Csx28 in the absence or presence of λ -phage infection (MOI of 0.1), respectively. In all cases, blots were first probed with either anti-HA or anti-V5 antibodies to detect HA-Cas13 and Csx28-V5, respectively, then probed for DnaK and OmpC as cytosolic and outer-membrane fractionation controls, respectively. IM, inner membrane; OM, outer membrane.

(E) A schematic detailing the mechanism by which DiBAC₄(3) detects membrane polarization. $\Delta\psi$, resting membrane potential. **(F)** Flow cytometry histograms of a DiBAC₄(3) staining assay measuring membrane depolarization of WT *E. coli* or *E. coli* possessing the indicated plasmids over the course of a λ -phage infection (MOI of 1). A polymyxin B (poly. B)-treated *E. coli* sample was used as a positive control for membrane depolarization. AU, arbitrary units. **(G)** Quantification of the percentage of depolarized cells in (F), determined by calculating the area under the curve of the depolarized-cell subpopulation as a percentage of the total population. **(H)** A schematic detailing the mechanism by which resazurin acts as a readout of cellular respiration. **(I)** Resazurin assay for untransformed *E. coli* or *E. coli* strains carrying the indicated plasmids in the absence or presence of λ -phage infection (MOI of 2). Data are shown as mean \pm SEM for three biological replicates. RFU, relative fluorescence units.



helices ($\alpha 3$ and $\alpha 4$) forming the outside of the pore (Fig. 2D). We conducted DALI (15), Foldseek (16), and 3D-surfer (17) structure similarity searches, as well as an Omakage (18) shape search, but found no deposited or AlphaFold-predicted structures of known function with structural similarity to Csx28.

The Csx28 protomers are arranged in a parallel head-to-head orientation (Fig. 2C) resulting in a pore lined with mostly positively charged amino acid side chains (Fig. 2E). These positively charged regions may provide selectivity toward specific ions or metabolites or act as potential nucleic-acid binding sites, especially given that Csx28 was previously predicted to contain a divergent HEPN motif (5). Canonical HEPN motif-containing proteins form “face-to-face” dimers that result in each HEPN motif facing toward another, lining a dimer interface that often forms an RNA-binding surface and/or ribonuclease (RNase) active site (19) (fig. S9). Whereas Csx28 adopts a four α -helical bundle fold common to HEPN motif-containing proteins, the oligomers form a “face-to-back” arrangement, which results in only one HEPN motif per interface rather than the expected two motifs. In our structure, only one of the predicted HEPN-motif (RX₄-H, where R is arginine, X is any residue, and H is histidine) residues, H157 (Fig. 2F), and a distinct set of conserved residues from a neighboring α helix and protomer (for example, Y55, Y104, T62, and R165, where Y is tyrosine and T is threonine) form the interface. The predicted HEPN motif arginine (R152), generally required for RNA hydrolysis, is oriented 180° away from the interface and forms a salt bridge with E122 (where E is glutamic acid) from helix $\alpha 2$ in the same protomer. In addition, in most HEPN domains, the HEPN motif resides at the junction between helix $\alpha 3$ and the $\alpha 3$ - $\alpha 4$ loop, whereas in our structure the predicted motif resides exclusively on helix $\alpha 4$. These observations suggest that Csx28 is either a very highly diverged HEPN domain protein that is not using its HEPN domain in a canonical sense or that Csx28’s fold is completely unrelated to HEPN domains. Both AlphaFold (20) and RoseTTA fold (21) predictions reveal a fold that is very similar to our cryo-EM-derived model (fig. S10, A to B), and furthermore, AlphaFold-Multimer (22) predicts a similar dimer interface arrangement, including side-chain positioning (fig. S10C), as well as a highly similar octameric arrangement (fig. S10D). We also observed that these features were conserved across the Csx28 tree, even at very low sequence identities (figs. S11 to S13, and supplementary text), providing further evidence that our cryo-EM model likely represents the major structural form of Csx28 found in nature.

To further probe whether the protomer-protomer interface was required for phage-

defense activity, we generated several single- and double-point mutations within Csx28's protomer-promoter interface. We found that single-point mutations in this region resulted in a ~2- to ~1400-fold reduction in λ -phage defense, and that in most cases double-point mutations could further exacerbate this effect (Fig. 2G). We also probed the importance of the R152: E122 salt bridge, which sequesters the predicted conserved HEPN arginine away from the interface. We observed that single-point mutants R152E (R152→E) and E122R (E122→R) result in a loss of Csx28-mediated λ -phage defense. However, combining these two mutations with the idea of reforming the salt bridge results in almost complete rescue in λ -phage defense (fig. S14), indicating that this salt bridge is important for the structure of the Csx28 protomer and its function in antiphage defense.

Csx28 is membrane localized in vivo and upon infection results in membrane depolarization and reduced metabolism

Given the pore-like structure observed in our cryo-EM analysis, we wondered how Csx28 may be affecting membrane function in vivo. We first wanted to observe the cellular localization of Csx28 and Cas13b expressed in *E. coli*. We tested a range of small epitope-tagged Csx28 and Cas13b constructs with EOP assays to ensure that tag addition did not affect the function of Csx28 and Cas13, and we found that a C-terminal V5 tag was optimal for Csx28 (fig. S15A), and that an N-terminal 3 \times hemagglutinin (HA) tag was optimal for Cas13b (fig. S15B). With these tagged proteins, we used membrane fractionation coupled with Western blotting to determine the localization of HA-Cas13b and Csx28-V5. HA-Cas13b was found to cofractionate with DnaK (a cytosolic chaperone) in the cytosol, whereas Csx28-V5 was found to reside exclusively in the DDM-soluble membrane fraction, cofractionating with OmpC (an outer membrane porin) (Fig. 3A). We went on to further explore whether Csx28 resides in the inner (cytosolic) membrane or the outer membrane and whether this localization depends on Cas13b and/or phage infection. Using additional fractionation of the inner and outer membranes, we observed that Csx28-V5 resides in the inner membrane regardless of Cas13b-crRNA1 expression (Fig. 3, B and C) or the absence (Fig. 3C) or presence (Fig. 3D) of λ -phage infection. These results indicate that Csx28 stably localizes in the inner membrane and that there are no large-scale changes in Csx28's localization dynamics during infection.

We next sought to observe any oligomeric dynamics of Csx28 in vivo and specifically whether these dynamics change in response to Cas13b expression and/or λ -phage infection. Cas13b- and Csx28-V5-expressing *E. coli* were

treated with a membrane-permeable protein cross-linker, disuccinimidyl suberate (DSS), before and after λ -phage infection, followed by Western blot analysis. We observed that Csx28 does exist as oligomers in *E. coli*, with a banding pattern that closely resembles the cross-linking of increasing multiples of Csx28 monomers up to larger, octameric-sized oligomers, with no substantial change in oligomerization upon Cas13b expression and/or phage infection (fig. S16A). We also harnessed a complementary glycerol gradient ultracentrifugation approach and observed that both before and after phage infection, Csx28 lies mostly in the middle of the gradient, indicative of stable oligomer formation (versus existing as a monomer exclusively, which would run at the top of the gradient) (fig. S16B). These results support the conclusion that the octameric form we observed in our cryo-EM structure likely exists in vivo independent of phage infection or the presence of Cas13b.

Observations of an octameric Csx28 pore-like membrane protein by cryo-EM, inner-membrane-localized Csx28 oligomer formation in vivo, and a slow-growing Cas13b:crRNA1-Csx28 phenotype during phage infection led us to wonder whether the Cas13b sensing of viral transcripts in the presence of Csx28 results in Csx28-mediated perturbation of the inner-membrane potential that exists in *E. coli*, a major contributor to the proton motive force (pmf), which *E. coli* use to drive the synthesis of adenosine triphosphate (ATP) and a range of transport processes (23). To test this hypothesis, we performed a flow cytometry-based membrane depolarization assay that uses bis-(1,3-dibutylbarbituric acid) trimethine oxonol [DiBAC₄(3)], which becomes fluorescent after accumulating in cells that have lost membrane potential (Fig. 3E) (24). We observed that in addition to our positive control, the known pmf disruptor polymyxin B, only phage-infected Cas13b:crRNA1- and Csx28-containing strains resulted in pronounced membrane depolarization with as much as 40% of the population depolarized at 90 min after infection (Fig. 3, F and G), whereas expression of Cas13b:crRNA1 (Fig. 3, F and G), Csx28, or Cas13b:ΔcrRNA (fig. S17A) alone did not result in any notable increases in membrane depolarization. To investigate whether this Cas13b-dependent, Csx28-dependent depolarization resulted in larger defects in membrane integrity, we performed propidium iodide (PI) staining and flow cytometry. PI requires gross defects in membrane integrity to enter the cell and emit fluorescence. We observed that Cas13b-dependent, Csx28-dependent membrane depolarization did not result in large changes in PI fluorescence relative to polymyxin B (fig. S17B), suggesting that the Csx28 membrane-pore structures formed in vivo cannot permeate PI. Given that PI is ~13 to 15 Å in size (short

and long axis, respectively), the lack of PI uptake is additional evidence that Csx28 pore diameters are likely strictly size-limited in vivo (to ~10 Å or less). Our membrane depolarization observations are in line with the slow-growing phenotype we observed, and with previous studies showing that *E. coli* can continue to grow after transient membrane depolarization (25, 26).

Phage propagation is an energy-intensive process for the host, and changes in host metabolic status can drastically affect phage-propagation dynamics (27). To further explore the downstream effects of membrane depolarization and dissipation of the pmf, we carried out resazurin assays to test whether Csx28-mediated membrane depolarization affects cellular metabolism and, ultimately, the potential for phage to propagate. Resazurin is a nonfluorescent substrate that is irreversibly converted by (reduced nicotinamide adenine dinucleotide) NADH- or (reduced nicotinamide adenine dinucleotide phosphate) NAPDH-dependent dehydrogenases to the fluorescent product resorufin in actively respiring cells that have sufficient NADH or NAPDH pools, and thus can be used to measure cellular respiration rates (Fig. 3H) (28). We observed that most of the cultures were able to completely metabolize resazurin to resorufin in ~300 min, even in the presence of a phage infection and the subsequent crash of the cell population. However, cultures containing Cas13b:crRNA1-Csx28 exhibited markedly different resazurin turnover kinetics, with two phases of noticeably slower turnover, requiring ~600 min to completely turn over resazurin (Fig. 3I and fig. S18). This much slower rate of resazurin turnover indicates a reduced rate of metabolism, likely caused by the dissipation of the pmf induced by Cas13b-induced, Csx28-dependent membrane depolarization. We hypothesize that an attenuated metabolic rate allows access to a cellular state that reduces the ability for phage to actively propagate. This phenomenon is similar to what is observed when λ -infected *E. coli* are treated with a pmf-collapsing membrane ionophore, carbonyl cyanide *m*-chlorophenyl hydrazone (CCCP): The infected *E. coli* fail to produce additional λ virions after exposure because of to the collapse of host-cell metabolism (29).

Csx28 interacts with RNA but not directly with an activated target bound Cas13b-RNA complex

Next, we wanted to further understand how Cas13b sensing of phage RNA could be communicated to Csx28 to modulate its function at the inner membrane. Given our earlier observation that Csx28 requires a nuclease-active, phage-targeting Cas13b to elicit enhanced defense (fig. S1), we first hypothesized that the RNA cleavage products generated by Cas13b

may bind to and modulate Csx28's function. Using RNA gel shift experiments, we observed that octameric but not monomeric Csx28 binds RNA with high affinity (fig. S19, A and B). To confirm this observation, we used ultraviolet cross-linking and observed that upon cross-linking and the presence of RNA, Csx28 forms covalently stabilized dimers and higher-order oligomers, confirming that Csx28 octamers can bind RNA (fig. S19C). These data also help explain why a Csx28 monomer is unable to bind RNA; the cross-linking suggests that RNA binding most likely occurs across the protomer-protomer interfaces of Csx28 oligomers. To further support our hypothesis that RNA cleavage products may have a role in Csx28 function, we wanted to confirm that Cas13b can cleave targeted RNA and whether Csx28 possesses any RNase activity or can boost Cas13b RNase activity as previously hypothesized (5). We first demonstrated that *in vitro*, purified Cas13b:crRNA possessed robust trans-ssRNA cleavage of a fluorescent RNA reporter upon target RNA binding, and that neither monomeric or octameric Csx28 cleaved the RNA reporter or helped to boost Cas13b's RNase activity (fig. S20A). *In vivo*, using length distribution analysis of extracted RNA, we observed subtle changes in the distributions of small RNA-sized species when Cas13b:crRNA1 alone is active (fig. S20, B to E, and supplementary text), indicating that tRNAs are likely being cleaved by Cas13b, as previously observed with Cas13a (30). To test an alternative hypothesis that Csx28's membrane-modulating activity is a result of a direct binding interaction with an active Cas13b:crRNA:target-RNA ternary complex, we carried out HA-Cas13:crRNA1 and Csx28-V5 immunoprecipitations in the absence and presence of λ -phage infection (fig. S21, A and B), as well as analytical size-exclusion experiments with purified Cas13b complexes and octameric Csx28 (fig. S21C), and in all cases could not detect a direct interaction between an active Cas13b:crRNA:target-RNA complex and Csx28; however, one cannot rule out that highly transient interactions between these two complexes may play a role in Csx28 function. On the basis of these findings, we propose the following hypothetical model of Csx28 function in Cas13b-sensed antiphage defense (fig. S22).

Discussion

Structurally, Csx28 represents a new class of membrane-pore protein because it has no noticeable structural similarity to any previously determined protein structures. Csx28 was also hypothesized to possess a divergent HEPN RNA-binding or RNase motif (3, 5–8); however, the HEPN-motif positioning on helix α 4 and the face-to-back protomer interface we observed suggest that this prediction is likely incorrect. The clear presence of a pore-channel-

like feature in our structure, mutagenesis highlighting the importance of this interface in Csx28 function, and observation of membrane depolarization that potentially links structure to function, lead us to suggest that the divergent face-to-back interface formed by Csx28 is the state required for antiphage defense. Our Csx28 structure also provides strong evidence that the N-terminal helix forms a functional transmembrane spanning region, the same region as correctly predicted by the membrane topology algorithm TMHMM (13). Functionally, Csx28 bears more similarity to other large-pore channel proteins [e.g., pannexins and connexins; for a review, see (14)], viroporins [for a review, see (31)], and cyclic nucleotide-gated ion channels [for a review, see (32)] than to phage holins or gasdermins with respect to their pore diameter and their lack of ability to grossly disrupt membrane function. This evidence explains the differences in downstream phenotype: transient membrane depolarization using size-limited and likely gated pore-channel-like structures versus large-scale membrane disruption through the formation of very large and dynamic oligomers, respectively. Our data indicate that rather than acting to stimulate the RNase activity of the associated Cas13b as previously hypothesized (5), Csx28 might act as a terminal effector in antiphage defense.

REFERENCES AND NOTES

- O. O. Abudayyeh *et al.*, *Science* **353**, aaf5573 (2016).
- A. East-Seletsky *et al.*, *Nature* **538**, 270–273 (2016).
- M. R. O'Connell, *J. Mol. Biol.* **431**, 66–87 (2019).
- A. J. Meeske, S. Nakandaki-Higa, L. A. Marraffini, *Nature* **570**, 241–245 (2019).
- A. A. Smargon *et al.*, *Mol. Cell* **65**, 618–630.e7 (2017).
- S. Shmakov *et al.*, *Nat. Rev. Microbiol.* **15**, 169–182 (2017).
- M. C. Pillon, J. Gordon, M. N. Frazier, R. E. Stanley, *Crit. Rev. Biochem. Mol. Biol.* **56**, 88–108 (2021).
- H. Shivram, B. F. Cress, G. J. Knott, J. A. Doudna, *Nat. Chem. Biol.* **17**, 10–19 (2021).
- W. X. Yan *et al.*, *Mol. Cell* **70**, 327–339.e5 (2018).
- V. Höikkälä *et al.*, *mBio* **12**, e03338-20 (2021).
- N. Toro, M. R. Mestre, F. Martínez-Abarca, A. González-Delgado, *Front. Microbiol.* **10**, 2160 (2019).
- S. Konermann *et al.*, *Cell* **173**, 665–676.e14 (2018).
- A. Krogh, B. Larsson, G. von Heijne, E. L. Sonnhammer, *J. Mol. Biol.* **305**, 567–580 (2001).
- J. Syrjanen, K. Michalski, T. Kawate, H. Furukawa, *J. Mol. Biol.* **433**, 166994 (2021).
- L. Holm, L. M. Laakso, *Nucleic Acids Res.* **44** (W1), W351–W355 (2016).
- M. van Kempen *et al.*, *bioRxiv* 2022.02.07.479398 [Preprint] (2022).
- T. Aderinwale *et al.*, *Commun. Biol.* **5**, 316 (2022).
- H. Suzuki, T. Kawabata, H. Nakamura, *Bioinformatics* **32**, 619–620 (2016).
- V. Anantharaman, K. S. Makarova, A. M. Burroughs, E. V. Koonin, L. Aravind, *Biol. Direct* **8**, 15 (2013).
- J. Jumper *et al.*, *Nature* **596**, 583–589 (2021).
- M. Baek *et al.*, *Science* **373**, 871–876 (2021).
- R. Evans *et al.*, *bioRxiv* 2021.10.04.463034 [Preprint] (2022).
- J. Stautz *et al.*, *J. Mol. Biol.* **433**, 166968 (2021).
- J. D. Te Winkel, D. A. Gray, K. H. Seistrup, L. W. Hamoen, H. Strahl, *Front. Cell Dev. Biol.* **4**, 29 (2016).
- F. M. Harold, J. Van Brunt, *Science* **197**, 372–373 (1977).
- N. Kinoshita, T. Unemoto, H. Kobayashi, *J. Bacteriol.* **160**, 1074–1077 (1984).
- E. W. Birch, N. A. Ruggero, M. W. Covert, *PLOS Comput. Biol.* **8**, e1002746 (2012).
- O. Braissant, M. Astasov-Frauenhoffer, T. Waltimo, G. Bonkat, *Front. Microbiol.* **11**, 547458 (2020).
- L. C. Thomason, D. L. Court, *FEMS Microbiol. Lett.* **363**, fnv244 (2016).
- I. Jain, *et al.*, tRNA anticodon cleavage by target-activated CRISPR-Cas13a effector. *bioRxiv* 2021.11.10.468108 [Preprint] (2021).
- J. L. Nieva, V. Madan, L. Carrasco, *Nat. Rev. Microbiol.* **10**, 563–574 (2012).
- L. M. R. Napolitano, V. Torre, A. Marchesi, *Pflugers Arch.* **473**, 1423–1435 (2021).

ACKNOWLEDGMENTS

We thank K. Awadya and N. Tong for insightful advice on experiments conducted for this manuscript and the O'Connell and Kellogg labs for helpful discussions. We thank M. Dumont for invaluable advice on membrane-protein purification and access to light scattering measurements; B. Adler for providing λ phage; C. Cavender for assistance with statistical analyses; and M. Cochran and the URM Flow Cytometry Resource for assistance with the flow cytometry experiments. We acknowledge the Center for Integrated Research Computing (CIRC) at the University of Rochester for computational resources and assistance and the support of National Institutes of Health (NIH) equipment grant S10-OD21489-01AI for the use of the Typhoon RGB Scanner. We thank the Cornell Center for Materials Research facility, as well as K. Spoth and M. Silvestry-Ramos, for maintenance of electron microscopes used for this research (NSF MRSEC program, grant DMR-1719875), and the Extreme Science and Engineering Discovery Environment (XSEDE) for computational resources used for image processing (MCB200090 to E.H.K.). We thank Sam Sternberg for critical feedback on the manuscript. **Funding:** This study was supported by NIH grant R35GM133462 (M.R.O.), NIH training grant T90 DE021985 (A.R.V.), NIH training grants T32 GM118283 and T32 GM145461 (A.R.V.), and NIH training grant T32 GM135134 (J.K.N.). **Author contributions:** M.R.O. and A.R.V. conceived the project. A.R.V. carried out the phage assays. A.R.V. carried out the colony formation and lysogeny assays with assistance from J.K.N. A.R.V. carried out protein purification. M.R.O. carried out the SEC-SLS experiments with assistance from A.R.V. J.-U.P. prepared samples for cryo-EM imaging; J.-U.P. analyzed, processed, and refined cryo-EM images to obtain 3D reconstructions; and J.-U.P. and E.H.K. built and refined atomic models. A.M.M.V. set up protein-structure predictions with assistance from M.R.O. A.R.V. and B.P. carried out the membrane fractionation and *in vivo* cross-linking experiments. A.R.V. carried out the flow cytometry experiments with assistance from M.R.O. A.R.V. carried out the resazurin experiments with assistance from M.R.O. A.M.M.V. carried out fluorescent RNA cleavage assays with assistance from A.R.V. M.R.O. carried out the analytical SEC experiments. M.R.O. and A.R.V. drafted the manuscript with input from J.-U.P., E.H.K., and B.P., and all authors synthesized the ideas, contributed to figures, and reviewed and edited the final manuscript. **Competing interests:** M.R.O. is an inventor on patent applications related to CRISPR-Cas systems and uses thereof. M.R.O. is a member of the scientific advisory boards for Dahlia Biosciences and LocanaBio and an equity holder in Dahlia Biosciences and LocanaBio. **Data and materials availability:** Atomic models are available through the Protein Data Bank (PDB) with accession codes 8G11 (Csx28). Cryo-EM reconstructions are available through the Electron Microscopy Data Bank (EMDB) with accession codes EMD-40059 (Csx28). Plasmids are being deposited on Addgene. **License information:** Copyright © 2023 the authors, some rights reserved; exclusive licensee American Association for the Advancement of Science. No claim to original US government works. <https://www.science.org/about/science-licenses/journal-article-reuse>

SUPPLEMENTARY MATERIALS

science.org/doi/10.1126/science.abm1184

Materials and Methods

Supplementary Text

Figs. S1 to S22

Tables S1 to S3

References (33–55)

MDAR Reproducibility Checklist

[View/request a protocol for this paper from Bio-protocol.](https://www.bio-protocol.org)

Submitted 20 October 2021; resubmitted 13 October 2022

Accepted 27 March 2023

10.1126/science.abm1184

Csx28 is a membrane pore that enhances CRISPR-Cas13b-dependent antiphage defense

Arica R. VanderWal, Jung-Un Park, Bogdan Polevoda, Julia K. Nicosia, Adrian M. Molina Vargas, Elizabeth H. Kellogg, and Mitchell R. O'Connell

Science, 380 (6643), .
DOI: 10.1126/science.abm1184

Editor's summary

In addition to containing RNA-guided nucleases, many CRISPR-Cas systems encode diverse accessory proteins that may help to bolster antiphage defense. Using a combination of cryo-electron microscopy, genetic, and biochemical approaches, VanderWal *et al.* discovered that Csx28, an accessory protein found in some CRISPR-Cas systems, forms an inner membrane-localized octameric pore. Upon Cas13 activation by viral messenger RNAs, Csx28 assists in protecting against sustained viral infection by helping to depolarize the inner membrane and slow metabolism. These findings expand the complexity of CRISPR-Cas-based defense systems and offer the potential for new molecular technologies. —Di Jiang

View the article online

<https://www.science.org/doi/10.1126/science.abm1184>

Permissions

<https://www.science.org/help/reprints-and-permissions>